

Possible surface plasmon polariton excitation under femtosecond laser irradiation of silicon

Thibault J.-Y. Derrien,^{1,2, a)} Tatiana E. Itina,¹ Rémi Torres,² Thierry Sarnet,² and Marc Sentis²

¹⁾Laboratoire Hubert Curien (LabHC), UMR CNRS 5516 - Université Jean-Monnet.

Bâtiment F, 18 rue du Professeur Benoit Lauras, F-42000 Saint-Etienne, France.

²⁾Laboratoire Lasers, Plasmas et Procédés Photoniques (LP3), UMR CNRS 7341 - Aix-Marseille Université, Parc Technologique et Scientifique de Luminy, Case 917, 163 avenue de Luminy, F-13288 Marseille CEDEX 09, France.

The mechanisms of ripple formation on silicon surface by femtosecond laser pulses are investigated. We demonstrate the transient evolution of the density of the excited free-carriers. As a result, the experimental conditions required for the excitation of surface plasmon polaritons are revealed. The periods of the resulting structures are then investigated as a function of laser parameters, such as the angle of incidence, laser fluence, and polarization. The obtained dependencies provide a way of better control over the properties of the periodic structures induced by femtosecond laser on the surface of a semiconductor material.

PACS numbers:

(68.47.Fg) Semiconductor-vacuum interface

(71.36.+c) Polaritons

(81.16 Rf) Micro and nanoscale pattern formation

I. INTRODUCTION

Femtosecond lasers are known to be powerful tools for micro- and nanomachining. In particular, these lasers can induce periodic modulations ("Laser-Induced Periodic Surface Structures" or LIPSS) on the surfaces of metals, semiconductors and dielectric samples at relatively moderate laser fluences¹⁻⁶. Furthermore, it is possible to decrease periods of these structures below the laser wavelength, thus rising the precision of laser nanomachining beyond the diffraction limit⁷⁻¹⁰. Applications of the ripple structures are numerous. For instance, it is possible to colorize metals and to control over laser marking^{11,12}.

For further development of these applications, it is important to better understand the mechanisms of ripple formation by femtosecond laser pulses. The number of the observed structures is, however, very large making the control over the laser parameters very complicated. In general, two types of structures can be distinguished (i) resonant structures, where the resulting period is correlated with laser wavelength, and (ii) non-resonant structures, which are not explicitly connected with the laser wavelength and with the coherent effects. Thus, the so-called Low-Spatially-Frequency LIPSS (LSFL) belong to the resonant structures⁸. In addition, much larger parallel ripples of several micrometers, can be considered to belong to the non-resonant structures. In this case, a large number of pulses is required to provide a thick melted depth comparable to the structure amplitude, so that these ripples are rather connected with the capillary wave generation or surface stress⁵. The non-resonant structures were also ex-

plained by the self-organized processes, described by the *Kuramoto-Sivashinsky* equation¹³⁻¹⁵. With the increase in laser pulses and fluence, drop-like structures named "beads", and then conical structures called "black silicon" can be also obtained^{4,16-19}.

In this paper, we focus our attention at the resonant periodic structures with the period near the laser wavelength e.g. the LSFL. The classical theory of ripple formation proposes that scattering of the laser wave by surface roughness couples the laser wave with the surface modes, which interfere with the laser light, and thus lead to a periodic modulation of the absorbed energy²⁰. This theory was recently confirmed by the numerical calculations based on the system of Maxwell equations for rough surface²¹. This scenario requires the presence of an initial roughness of a certain size. Both the laser parameters and the surface roughness are, however, often unknown. In addition, several laser pulses are frequently required to form a structure. In this case, the period of the energy deposition can be smaller than laser wavelength, as was explained by Bonse et al²² by using the "Sipe-Drude" model. In this way, an explanation of the very narrow structures (HSFL) appearing after numerous pulses^{23,24} was proposed. In addition, Tsibidis et al.²⁵ recently investigated the cumulative hydrodynamic effects and the corresponding surface modifications. It was found that a non-resonant mechanism explains the reduction of the LSFL periodicity with the increase of pulse number in Si. In addition, the possibility to create periodic surface modifications with a single femtosecond pulse was demonstrated for metals and semiconductor materials^{18,22,26}. To explain the formation of the near-wavelength ripples at intense and reduced number of pulses, several authors have proposed the surface plasmon polaritons (SPP) as the mechanism responsible for the surface wave generation in semiconductors and dielectrics^{22,27,28}. The sur-

^{a)}Electronic mail: thibault.derrien@gmail.com

face plasmon polaritons are known to be excited on metal surfaces. The ripple formation mechanism for metals has been linked with the excitation of surface plasmon polariton by several authors^{29,30}. However, the excitation conditions remain rather puzzling in the case of semiconductor or dielectric materials. Moreover, it is not clear if the SPP coupling can occur by using a single femtosecond laser pulse, since specific coupling conditions are required to add the missing momentum at the surface. In particular, gratings, snom probe, prism, defects, or roughness^{31,32} typically help to couple the laser wave with a surface wave mode. Thus, our study focuses on the semiconductor case, and the analyzed material is monocrystalline Si.

In the case of semiconductor materials, laser-induced modification of the dielectric function changes material properties. As a result, the importance of a transitory metallic state was underlined by Bonse et al³³. In such cases, however, the presence of a nanometric defect (such as bubbles or nanoparticle) at the surface is required and those methods correspond to the well-known case of localized surface plasmon (LSP) excitation around isolated defects³⁴. It was demonstrated, furthermore, that the transient modification of the solid properties follows the plasma dynamics of the free-carrier gas, due to their excitation by the intense laser^{35,36}. However, a systematic study is still required for the conditions of SPP excitation on semiconductor surface by a femtosecond laser interaction. Under these excitation, electron-hole pairs are generated, but also thermal effects play a role. That is why a clear explanation is required for the laser parameter range, ambient environment and sample surface conditions. To help developing the corresponding applications, the resulting ripple periods should be connected with laser parameters. In this paper, we consider the conditions required to excite surface plasmon polaritons on semiconductor's surface. The developed model provides all the parameters, which lead to the SPP excitation, such as angle of incidence, laser fluence, pulse duration, and surface roughness for the given ambient optical properties. It is demonstrated that, under the required conditions, Si surface becomes optically active under femtosecond irradiation, and thus, SPPs can be excited by irradiation of a coupling device. The resulting periods are analyzed as a function of laser parameters.

The paper is organized as follows. In Section II, we present the experimental protocol. In Section III, we present the model and consider the modification of the optical properties of Si under femtosecond irradiation. In Section IV, conditions of the excitations of the surface plasmon polaritons are presented. In Section V, the laser parameters allowing the SPP excitation are examined as a function of laser fluence and laser pulse duration. Then, the required minimal roughness thickness is discussed. Finally, the calculated periodicities are compared to the experimental values as a function of laser fluence. The evolution of the ripple period is analyzed as a function of angle of incidence and laser polarization.

II. EXPERIMENTAL DETAILS

The micromachining experiments were performed by using a Ti-sapphire laser (Hurricane model, Spectra-Physics) that was operated at 800 nm, with an energy of 500 μJ , a repetition rate of 1 kHz and a laser pulse duration of 100 fs. Laser irradiation of silicon surface was carried out in a vacuum system with a pressure of 5×10^{-5} to 1×10^{-5} mbar. This low pressure considerably reduces the redeposition of unwanted debris from the laser ablation process. To get a more uniform laser energy distribution, only the center part of the gaussian laser beam was selected using a square mask of $2 \times 2 \text{ mm}^2$. A spot about $35 \times 35 \mu\text{m}^2$ area was obtained projecting the mask image onto the sample surface with a lens ($f' = 50 \text{ mm}$). Laser beam was perpendicular to the sample surface. In the present study, we consider only linear polarization. The laser energy delivered to the sample surface could be attenuated by coupling an analyzer and a polarizer and completed by a set of neutral density filters. The analyzer rotation placed in front of the polarizer is controlled by a computer. The engraving results are in situ monitored by a CCD camera. The number of pulses is controlled by triggering a Pockels cell, thus reducing the repetition rate of the laser pulse to 5 Hz. We irradiated a $\langle 100 \rangle$ monocrystalline silicon (c-Si) wafer by one or several laser pulses at fluences of 0.5 J/cm^2 , 0.8 J/cm^2 , and 1.15 J/cm^2 . Two series of experiments were performed. (i) At very low (one or two) number of pulses, the angle of incidence has been kept normal to the surface. (ii) At $N = 10$ pulses, the angle of incidence and the laser polarization have been varied.

III. MODELING DETAILS

Femtosecond laser can promote carriers from the valence band of a semiconductor to the conduction band leading to free-carrier absorption. In our model, the number density of the carriers in the conduction band is calculated by solving the following equation

$$\frac{\partial n_e}{\partial t} - \nabla \cdot (k_B T_e \mu_e \nabla n_e) = G_e - R_e \quad (1)$$

where n_e is free-carriers number density, and $G_e = \left[\frac{\sigma_1 I}{\hbar \omega} + \frac{\sigma_2 I^2}{2\hbar \omega} + \delta_I n_e \right] \frac{n_v}{n_e + n_v}$ is the gain of free-carriers per unit time and unit volume ($\text{m}^{-3} \cdot \text{s}^{-1}$). n_v is the quantity of valence band electrons.

Both one-photon interband cross-section (σ_1) and the two-photon cross-section (σ_2) are used in the model (Table I). The conduction band can be also populated due to the electron impact ionization (avalanche process). The corresponding coefficient δ_I is also given in Table I. $R_e = \frac{n_e}{\tau_0 + \frac{1}{C n_e^2}}$ is the loss of conduction electrons by Auger recombination, where the recombination time τ_0 is equal to 6 ps in our calculations^{37,44}.

Physical meaning	Notation	Value	Unit	Reference
One-photon absorption coefficient	σ_1	$2\omega Im\sqrt{\varepsilon_\infty(\omega)}/c = 1.021 \times 10^5$	m^{-1}	(d, g)
Two-photon ionization rate	σ_2	0.1×10^{-9}	$m.W^{-1}$	(c)
Impact ionization probability rate	δ_I	$3.6 \times 10^{10} e^{-E_g/k_B T_e}$	s^{-1}	(b, e, f)
Auger recombination rate	C	3.8×10^{-43}	$m^6.s^{-1}$	(b)
Recombination delay at high density	τ_0	6	ps	(a)

TABLE I: The calculation parameters for c-Si under 800 nm irradiation. References: (a) Ref.³⁷, (b) Ref.³⁸, (c) Ref.³⁹, (d) Ref.⁴⁰, (e) Ref.⁴¹, (f) Ref.⁴², (g) Ref.⁴³.

The initial density of free-carriers present in the conduction band is $1.84 \times 10^9 cm^{-3}$ at a temperature of 300 K. k_B is the Boltzmann constant. In the near-ablation regime, using low energy photons (1.5 eV in our case), the number of excitable electrons is limited to the ones available in the valence band. Even in ablation regime at the considered laser intensities, less than one electron per atom is usually promoted to the conduction band⁴⁴. Thus, the number of the excitable valence band electrons is described by $n_0 = \rho_{Si} = 5 \times 10^{22} cm^{-3}$, equal to the density of the Si lattice. During the excitation, the number of valence band electrons n_v is therefore calculated by $n_v = n_0 - n_e$.

The free-carrier mobility is described by $\mu_e = \frac{e}{m_e \nu}$ where $\nu = 1.5 \times 10^{14} s^{-1}$ is the free-carrier collision frequency. Collision frequency is adjusted in agreement with melting fluence and melted depth given by Bonse et al⁴⁵, consistent with Monte Carlo simulations of collision frequency in Si⁴⁶. m_e is the optical mass of electron-hole pairs, which is equal to³⁶ $m_e = 0.18m_{e0}$, where m_{e0} is the electron mass. The density of electrons is calculated by using Eq. (1) taking into account thermal diffusion and Auger recombination. The hole temperature and density are considered equal to the ones of free-electrons, since the contribution of the electron-hole pairs to the absorption is taken into account by the optical mass in dielectric function.

Laser energy absorption is calculated as follows^{38,44}

$$\frac{\partial I}{\partial z} = -\alpha_{fcr} I - (\sigma_1 I + \sigma_2 I^2) \frac{n_v}{n_e + n_v}, \quad (2)$$

where I is the local intensity. Intensity at the surface is given by $I_{z=0}(t, x) = [1 - R(x)] I_0(t, x) \frac{1}{\cos \theta}$ and $I_0(t, x) = \frac{2F}{\tau} \sqrt{\frac{\ln(2)}{\pi}} e^{-\frac{1}{2}(\frac{x}{\sigma_x})^2} e^{-\frac{1}{2}(\frac{t-t_0}{\sigma_\tau})^2}$. F denotes the maximum fluence reached during the interaction. $t_0 = 0$ in our calculations. Spot size w_0 and pulse duration τ are respectively defined at the FWHM of spatial and temporal gaussian distributions. Thus, $\sigma_x = \frac{w_0}{2\sqrt{2 \ln 2}}$ and $\sigma_\tau = \frac{\tau}{2\sqrt{2 \ln 2}}$. The free-carrier absorption is described by $\alpha_{fcr} = \frac{2\omega n_2}{c}$ where

$$n_2 = \sqrt{0.5 \left(-\Re(\varepsilon_{fcr}) + \sqrt{\Re(\varepsilon_{fcr})^2 + \Im(\varepsilon_{fcr})^2} \right)}$$

and $\varepsilon_{fcr} = 1 - \frac{\omega_p^2}{\omega^2} \frac{1}{1+i\frac{\nu}{\omega}}$ describes the dielectric response

of the free-carriers.

During the interaction, the surface reflectivity changes depending on the angle of incidence θ and on laser polarization. In the present study, we consider only linear laser polarization.

We take into account the contribution of each layer to the surface reflectivity. The simulated region is considered as a layered structure where each layer j has its own optical properties related to the local free-carrier density. The layer thickness h_j coincides with the numerical cell width. The fraction of the plain wave amplitude reflected by the layers from j to k is calculated by the recurrence formula

$$r_{j,k} = \frac{r_{j,j+1} + r_{j+1,k} e^{2i\phi_{j+1}}}{1 + r_{j,j+1} r_{j+1,k} e^{2i\phi_{j+1}}}.$$

The final value of the surface reflection coefficient R is determined as $R = |r_{0,N}|^2$ where 0 corresponds to the sample-vacuum interface (with optical properties of the environment) and N is a layer located deep in the substrate. $\phi_{j+1} = \frac{2\pi h_{j+1}}{\lambda} \sqrt{\varepsilon_{j+1}}$ is the phase shift induced by the $j+1$ layer, h_{j+1} is the thickness of the layer $j+1$. $r_{j,j+1}$ is given by Fresnel equations.⁵⁰ ε_j is the full dielectric function given by Eq. (3) calculated at the layer j . The dielectric function is calculated as follows^{36,44}

$$\varepsilon_{Si}(\omega, n_e, \nu) = 1 + (\varepsilon_\infty(\omega) - 1) \frac{n_v}{n_e + n_v} - \frac{\omega_p^2}{\omega^2 (1 + i\frac{\nu}{\omega})} \quad (3)$$

where $\varepsilon_\infty(\omega)$ is the dielectric constant and depends on laser wavelength⁴⁰. ω_p is the plasma pulsation defined here by $\omega_p^2 = \frac{n_e e^2}{m_e \varepsilon_0}$. ω is the laser pulsation defined by $\omega = \frac{2\pi c}{\lambda}$. Photo-emission and thermo-emission are neglected, since Dumber field strongly limits the transport and thus the loss of free-carriers at the surface.^{44,49}

Several parameters of the above model depend on temperature. Under femtosecond laser irradiation, the electron-hole sub-system is excited to much higher temperatures and electron heat conductivity is much larger than that of lattice. To calculate temperatures of carriers and lattice, a two-temperature model is used. The laser-excited zone is small, so that ballistic effects should be also accounted for the electron sub-system. Therefore, we use the following ballistic-diffusive equation⁵¹⁻⁵³ to describe the electron-hole subsystem.

$$\frac{1}{4\nu} \frac{\partial^2 T_e}{\partial t^2} + \frac{\partial T_e}{\partial t} = \nabla (D_{SBD} \nabla T_e) - \frac{\gamma_{ei}}{C_e} (T_e - T_i) + \frac{Q_e}{C_e},$$

where $D_{SBD} = \frac{L^2 \nu}{6\pi^2} [\sqrt{1 + 4\pi^2 K n^2} - 1]$ is the effective free-carrier thermal diffusion term, based on the ratio $Kn = \frac{l_{MFP}}{L}$ of free-carrier mean-free-path $l_{MFP} = \frac{1}{\nu} \sqrt{\frac{3k_B T_e}{m_e}}$ and size of the excited zone $L \sim (2\omega \Im m \sqrt{\epsilon_{Si}}/c)^{-1}$. Specific heat capacity of free-carriers is taken to be equal to the classical limit $C_e = \frac{3}{2} k_B n_e$. The source term $Q_e = \left[(\hbar\omega - E_g) \frac{\sigma_1 I}{\hbar\omega} + (2\hbar\omega - E_g) \frac{\sigma_2 I^2}{2\hbar\omega} - E_g \delta I n_e \right] \frac{n_0 - n_e}{n_0} + \alpha_{fcr} I + E_g R_e - \frac{3}{2} k_B T_e \frac{\partial n_e}{\partial t}$ describes the energy of free-carriers by taking into account one-photon and two-photon ionization, the energy loss by electron avalanche, the free-carrier heating, the release of energy due to Auger recombination and last term comes from the variation of the specific heat capacity with time, since density is strongly modified during the pulse.

The time of free-carrier coupling to the lattice was experimentally determined by Sjodin et al³⁹ as a function of free-electron density given by $\tau_\gamma = \tau_{\gamma 0} \left[1 + \left(\frac{n_e}{n_{th}} \right)^2 \right]$ with $n_{th} = 6.02 \times 10^{20} \text{ cm}^{-3}$ and $\tau_{\gamma 0} = 240 \text{ fs}$. In our calculations, the coupling rate is given by⁴⁴ $\gamma_{ei} = \frac{C_e}{\tau_\gamma}$. Because of the slow thermal diffusion of the lattice energy, we describe the temperature of the lattice T_{Si} by a classical diffusion equation, taking into account the energy transferred from free-carriers as follows

$$C_{Si} \frac{\partial T_{Si}}{\partial t} = \nabla (\kappa_{Si} \nabla T_{Si}) + \gamma_{ei} (T_e - T_{Si})$$

The specific heat capacity of Si is a function of liquid density fraction. For solid state, dependence with temperature is given by relations³⁸ $C_{s-Si} [J.m^{-3}] = 10^6 [1.978 + 3.54 \times 10^{-4} T - 3.68 T^{-2}]$ and $\kappa_{s-Si} [W/m/K] = 10^2 [1585 T^{-1.23}]$. For liquid state, parameters are given by⁵⁴⁻⁵⁶ $C_{l-Si}(T) = 1.045 \times 10^3 \rho_{l-Si}$, where $\rho_{l-Si} = 2520 \text{ kg/m}^3$ and $\kappa_{l-Si}(T) = 10^2 [0.502 + 29.3 \times 10^{-5} (T - T_m)]$. Melting temperature T_m depends on the free-electron density as described by Eq. (4). During the phase transition, both Si heat capacity and conductivity are calculated using the fraction of liquid η , and are respectively defined by $C_{Si}(T) = (1 - \eta) C_{s-Si}(T) + \eta C_{l-Si}(T)$ and $\kappa_{Si}(T) = (1 - \eta) \kappa_{s-Si}(T) + \eta \kappa_{l-Si}(T)$. Melting is considered by using melting enthalpy ΔH_m at the melting temperature T_m . The resulting thermal energy is given by $U = \int_{T_0}^{T_m} C_{s-Si}(T') dT' + \Delta H_m + \int_{T_m}^T C_{l-Si}(T') dT'$ where U is the internal energy of the lattice, T is the Si temperature, $T_0 = 300 \text{ K}$ is the initial temperature of the system, and $\Delta H_m = 4 \times 10^9 \text{ J/m}^3$ is the melting enthalpy of Si.

Previously, two different types of phase transitions were shown to take place for Si⁵⁷⁻⁵⁹. The first one is

thermal melting and is described by a thermal criterion based on the required energy $E_m = k_B T_m \rho_{Si} + \Delta H_m$. The second phase transition mechanism is a so-called "non-thermal melting" due to the lattice decomposition due to a large number of carriers in the conduction band. The contribution of the non-thermal melting is also taken into account by the decrease of the band gap energy as a function of free-carrier density³⁸ (limited to positive or null values) expressed by $E_g(T, n_e) = 1.17 - 4.73 \times 10^{-4} \frac{T^2}{T+636} - 1.5 \times 10^{-10} n_e^{1/3}$ and by a lowering of the melting temperature described by the relation⁶⁰

$$T_m = T_m^0 - \frac{n_e E_{gap}}{C_{s-Si}} \quad (4)$$

where $T_m^0 = 1687 \text{ K}$.

Boundary conditions for transport equations are set so that free-carriers do not leave the sample. The sample is 250 μm thick, and the optical transmission has been checked to be zero through the sample.

IV. SURFACE PLASMON POLARITONS

Light can be coupled from free space into the surface plasmon polaritons (SPP) only by matching the momentum of the SPPs. This can be done via index matching³¹, or grating coupling^{61,62}. In addition, other cases can be considered. A non-resonant excitation can be performed by scattering of the laser wave on surface defects or a surface roughness. In such a case, laser wave is scattered on a broad angular distribution, and a part of the laser energy couples with surface modes. Laser wave can also interact with near-wavelength structures as described by Mie scattering, which leads to the excitation of localized surface plasmons (LSP)^{34,63}.

In each case, the excitation of surface waves requires several resonance conditions^{31,32,64}. In this part, we present theoretical conditions allowing the excitation of the Surface Plasmon Polaritons (SPPs) at the laser-irradiated surface of Si.

The excitation conditions of surface plasmon polaritons at a flat surface is that the corresponding curves cross in the dispersion diagram^{31,64}. The dispersion relation is obtained from the boundary conditions of the electric and magnetic field at the interface. The continuity of the electric field at the interface results to the expression $\frac{k_2}{k_1} = -\frac{\epsilon_2}{\epsilon_1}$, where $\epsilon_{1,2}$ are the dielectric constants on both sides of the interface, and $k_{1,2}$ are the respecting momenta of the both sides of the interface. In the general case, this expression can be verified only if

$$\Re(\epsilon_1) \Re(\epsilon_2) < 0 \quad (5)$$

which corresponds to a metal-dielectric interface. The continuity of the magnetic field at the interface leads to the expression of the SPP wave-number

$$\beta = \frac{\omega}{c} \sqrt{\frac{\epsilon_1 \epsilon_2}{\epsilon_1 + \epsilon_2}} \quad (6)$$

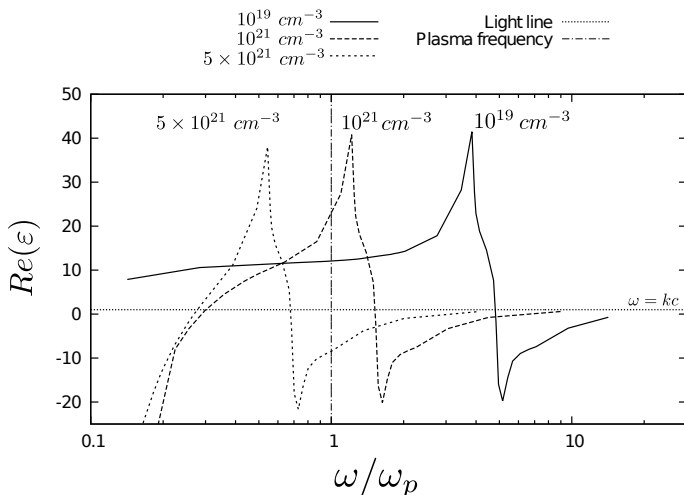


FIG. 1: Real part of the dielectric function of Si $\epsilon(\omega) = \left(\frac{kc}{\omega}\right)^2$ as a function of photon energy compared to the plasma frequency $\omega_p = \sqrt{\frac{n_e e^2}{m_e \epsilon_0}}$. If the plasma frequency is located on the left of the resonance peak, surface mode is not bounded to the surface and SPP are not allowed. If the plasma frequency is located on the right of the surface plasmon polariton resonance peak, the SPPs are allowed.

and to a second SPP excitation condition given by:

$$\Re(\epsilon_2) < -\Re(\epsilon_1) \quad (7)$$

By introducing Eq. (3) into Eq. (6) and considering an interface with vacuum ($\epsilon_1 = 1$), we calculate the dispersion relation as a function of free-carrier density. Figure 1 presents the dispersion relation of Surface Plasmon Polariton and laser wave in the case of Si, as a function of laser frequency, normalized to plasma frequency. In this calculation, the band structure of Si has been taken into account by replacing $\epsilon_\infty(\omega)$ in Eq. (3) following the measurements of Palik⁴⁰. The wave-vector k is squared and normalized to the laser pulsation to obtain the dielectric function, and is presented as a function of pulsation ω . The dispersion curve of the SPP reveals a plasmon resonance of the free-carrier plasma if the plasma frequency is comparable with the laser frequency e.g. if the free-carrier density is high. In the case of a doped semiconductor near the eigenfrequency, the intersection of the dispersion curves is possible³¹. In the case of femtosecond laser interaction, similarly, laser-induced ionization provides free-carrier contribution to the dielectric function, which is equivalent to a transient doping. Therefore, the intersection also becomes possible. The bounding of the coupled wave to the surface is described by the condition $\omega < \frac{\omega_p}{\sqrt{2}}$ in a perfect conductor⁶⁵. In the case of damped material, however, the leaky part of the dispersion relation between $\omega_{spp} = \frac{\omega_p}{\sqrt{2}}$ and ω_p is allowed⁶⁴. The condition on pulsation in a damped material is thus

described by

$$\omega < \omega_p. \quad (8)$$

The minimal density leading to satisfy this latter condition is the critical density at which $\Re(\epsilon) = 0$.

The coupling of far field laser wave with the SPP is also possible in the case of a surface with defects or roughness³¹. In this case, the pseudo-grating period has a large thickness δk around its average value, and leads to a small but non-zero coupling efficiency. Because of the laser irradiation, a coupling of a few percent is sufficient to obtain a periodic modulation of the deposited energy by interference between laser and SPP waves²⁸.

Finally, the conditions to satisfy (Eq. 5, Eq. 7, and Eq. 8) allowing the excitation of the SPP at the vacuum-Si interface can be combined into the condition:

$$\Re(\epsilon) < -1 \quad (9)$$

This criterion corresponds to a minimal free-carrier density given by $N_e = 4.61 \times 10^{21} \text{ cm}^{-3}$ in the case of a laser irradiation of Si using a wavelength of $\lambda = 800 \text{ nm}$. Then, we determine laser parameters for which this condition is justified.

V. RESULTS AND DISCUSSION

A. Conditions for SPP excitation on Si

We now demonstrate that excitation of Surface Plasmon Polariton is possible on Si under femtosecond laser irradiation, and calculate the laser parameters leading to satisfy the surface plasmon polariton conditions.

We now demonstrate that excitation of Surface Plasmon Polariton is possible on Si under femtosecond laser irradiation, and calculate the laser parameters leading to satisfy the surface plasmon polariton conditions.

Figure 2 (a) shows the maximum of the free-carrier density as a function of laser fluence. At short pulse duration, the maximum free-carrier density is non-linear as a function of fluence. These results are explained by the fact that free carrier absorption of Si strongly depends on the carrier concentration with a resonance at the so-called critical density⁶⁶. The corresponding density in a solid is defined by the non-propagation condition $\Re(\epsilon_{Si}) = 0$, which gives $n_{cr} = \frac{m_e \epsilon_0 \epsilon_\infty (\omega^2 + \nu^2)}{e^2}$. If the collision frequency $\nu = 1.5 \times 10^{14} \text{ s}^{-1}$ is small compared to laser frequency at 800 nm wavelength $\omega = 2.35 \times 10^{15} \text{ s}^{-1}$, then, the critical density can be expressed as $n_{cr} = \frac{m_e \epsilon_0 \epsilon_\infty \omega^2}{e^2}$.^{36,66,67} At low laser intensity, the maximum density increases linearly, since the absorption is linear in this regime. Below critical density, one observes that the efficiency of the absorption increases, which is due to the significant contribution of the multiphotonic excitation. Above the critical density, absorption becomes limited by the surface reflectivity. Above

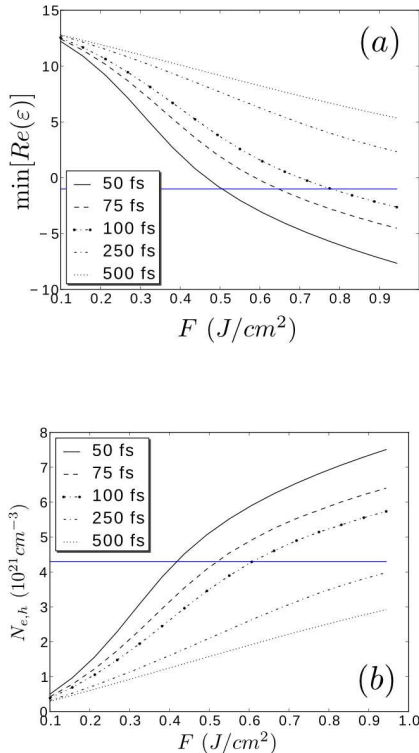


FIG. 2: (a) Minimum of the real part of the dielectric function as a function of laser fluence. Blue line indicates the threshold for SPP excitation e.g. $\Re(\varepsilon) = -1$. (b) Maximum of the reached density during the interaction as a function of laser fluence. Blue line indicates critical density e.g. $\Re(\varepsilon) = 0$. $n_{cr} = 4.29 \times 10^{21} cm^{-3}$. Several laser pulse durations are represented.

this limit, the number of free-carriers still increases due to high temperature of the free-carriers, leading to an interplay between diffusive transport and impact ionization.

Figure 2 (b) shows that the resonance condition is not met during the irradiation with a long pulse duration at the considered fluences, since the quantity of free-carriers is limited by the low intensity. It is shown that the real dielectric function decreases linearly if laser fluence is near the modification threshold ($0.2 J/cm^2$, see Refs^{45,68,69}). We observe that the critical density is not reached in this fluence regime. The difference with Ref³⁶ is explained by the different collision time, the two-photon cross section which is 10 times lower here (see Ref⁷⁰), and the impact ionization that we took into account. In the case of 100

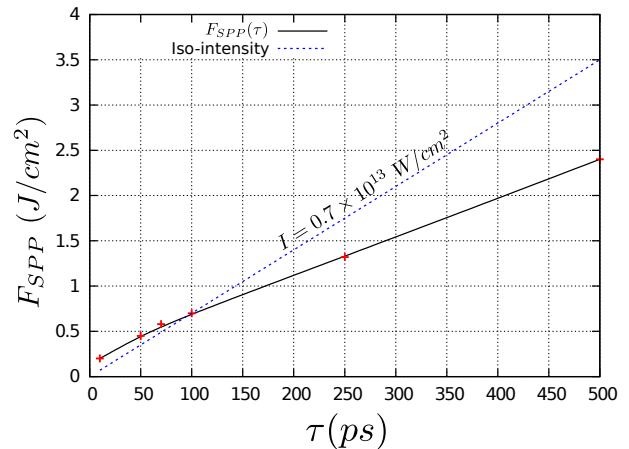


FIG. 3: Fluence threshold for SPP resonance as a function of pulse duration.

fs pulse duration, the condition given by Eq. (9) is satisfied above laser fluence of $0.7 J/cm^2$. A threshold for the excitation of SPP is then identified for a laser fluence of $0.7 J/cm^2$, a pulse duration of $\tau = 100$ fs, and a laser wavelength of $\lambda = 800$ nm. It is also shown that under shorter laser interaction, the condition for surface plasmon polariton excited is satisfied from lower fluences e.g. at $0.5 J/cm^2$ if $\tau = 50$ fs and $\lambda = 800$ nm.

From those results, a threshold fluence for SPP resonance can be defined for each pulse duration, above which the SPP resonance conditions are met. This result explains why a high fluence is necessary to induce the formation of periodic structures in single pulse experiments^{4,26,68}, since it results in a sufficient quantity of free-carriers to excite surface waves at the surface of Silicon.

In Figure 3, we demonstrate the fluence threshold for the SPP resonance as a function of laser pulse duration. The corresponding intensity, at which resonance occurs for 100 fs pulse, is shown by the dashed curve. By comparison of the curves, we observe that the required intensity for the SPP resonance increases with the decay in the laser pulse duration. This effect is due to the screening and large density gradient at the surface resulting into a strong diffusive transport.

Next we calculate the lifetime and the depth of the optically active zone, e.g. the distance under the surface where the sufficient number of free carriers are excited. Figure 4 shows the real part of the dielectric function as a function of time and depth. It is shown that under 50 fs pulse duration, at a fluence of $0.62 J/cm^2$, the excited zone is nearly 20 nm deep and the SPP excitation is allowed during a picosecond, which is greater than the pulse duration, thus leading to the excitation of SPPs in a shorter timescale than necessary for surface melting. Moreover, the damping length of the SPP is given by the relation^{31,64} $L_{SPP} = [2\Im m(\beta)]^{-1}$. The value of the damping length is contained between 500 nm and 2 μm if the SPP resonance conditions are met. Then,

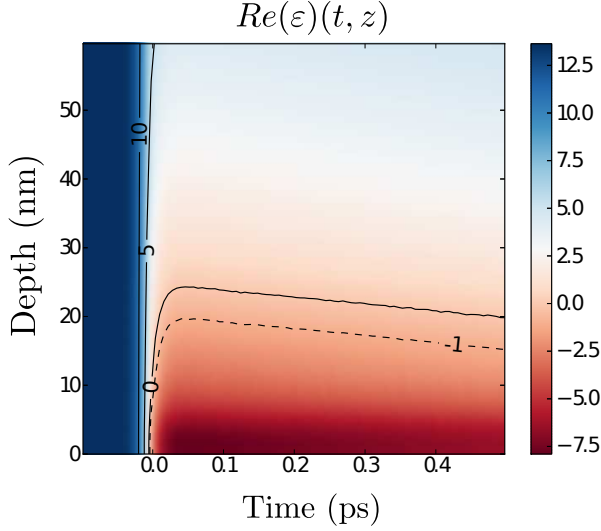


FIG. 4: Distribution of the dielectric function as a function of depth and time. $\tau = 50$ fs, $F = 0.62$ J/cm².

the excited SPPs propagate through several micrometers and can lead to periodic modulation if laser interferes with the SPPs, as experimentally observed around defects^{4,22,26,71,72}.

As underlined in the previous section, the phase-matching is possible at the surface of Si by using a scattering configuration with a defect or a roughness. We separate the following cases (i) the case of the roughness, for which the size of the scattering center is very small compared to the laser wavelength, and (ii) the case of a defect, for which the size is comparable to the laser wavelength. Both situations can lead to the excitation of Surface Plasmon Polariton if the conditions on the dielectric function are justified.

Figure 5 shows the distribution of the time-averaged transmitted field amplitude and normalized by the incident laser field intensity at the bottom of the selvedge region. This result has been calculated using the FDTD simulation package Lumerical⁷³ by irradiating a randomly generated rough Si surface using several control parameters: FWHM of the amplitude, and distance between the scattering centers. In this calculation, the roughness amplitude is distributed as a gaussian function between 0 and 15 nm. The distance between scattering centers is taken equal to 100 nm so that the scattered waves interfere together. The Si dielectric constant is taken equal to the value under 800 nm wavelength laser irradiation, in the case of low laser excitation. One observes that the amplitude of the field transmitted below the roughness is modulated if roughness amplitude is greater than 8 nm. Such a roughness is formed after a single laser pulse⁷⁴ at 0.5 J/cm². Thus, the amplitude allowing the coupling of surface waves with laser is 8 nm, which explains why strictly parallel ripples are observed after two pulses or more. Conversely, the formation of single pulse periodic structures is due to scattering on a

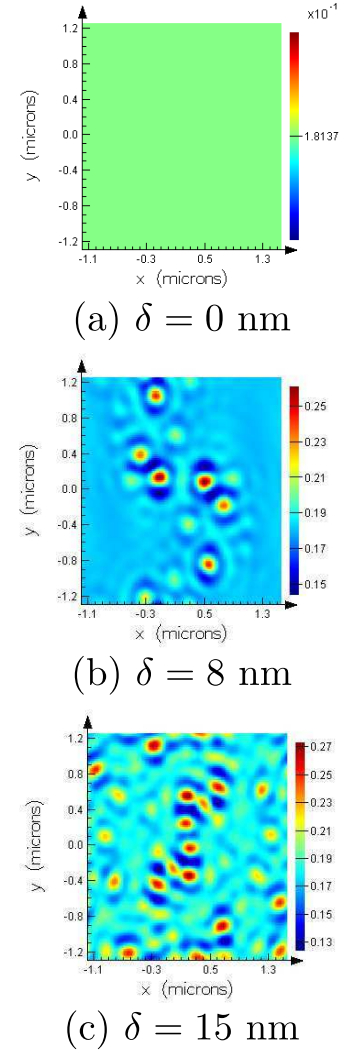


FIG. 5: Transmitted field amplitude below the selvedge region of Si. Roughness amplitude is (a) $\delta = 0$ nm, (b) $\delta = 8$ nm, (c) $\delta = 15$ nm at wavelength 800 nm. In these simulations, $\epsilon = \epsilon_\infty = 13.64 + 0.048i$.

near-wavelength defect, which leads to the excitation of Localized Surface Plasmon Polaritons distributed around scattering centers as observed by several authors^{22,26,71}. High fluence single pulse experiments leads to the formation of concentric structures rather oriented in the direction perpendicular to the laser polarization.

In this section, we have theoretically demonstrated that the excitation of Surface Plasmon Polaritons occurs on Si irradiated by femtosecond lasers. The excitation conditions are satisfied during the laser pulse if the laser intensity is high. At 50 fs pulse duration, a layer of about 20 nm becomes optically active and has a lifetime longer than the pulse duration. We turn now to the study of the period of the SPPs excited during ultrashort laser pulse on Si.

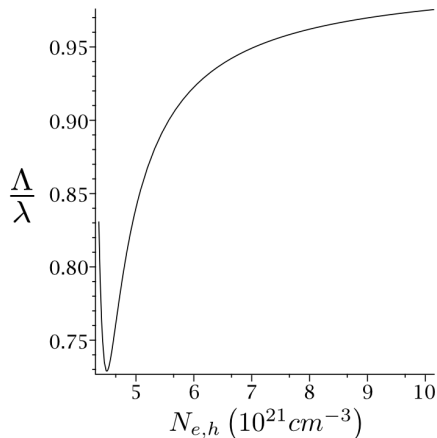


FIG. 6: Wavelength normalized period of SPP as a function of free-carrier density at vacuum - Si interface when the conditions of resonance are met.

B. Effect of the experimental parameters on SPP period

The SPP period dependency on laser intensity depends on the free-carrier density as follows

$$\Lambda = \frac{\lambda}{\sqrt{\frac{\varepsilon_1 \varepsilon_2(\omega)}{\varepsilon_1 + \varepsilon_2(\omega)}}}$$

where ε_1 and $\varepsilon_2(\omega)$ are respectively the dielectric functions of the media at both sides of the vacuum - Si interface. By substituting $\varepsilon_2(\omega)$ with Eq. (3), the periodicity of the SPP as a function of free-carrier density is calculated.

Figure 6 demonstrates the period of the SPPs at the vacuum - Si interface as a function of the free-carrier density. The values are presented for the free carrier number densities required for the SPP excitation. The resulting period varies considerably with the carrier density. The period of the SPPs is contained between 0.7λ and λ , which correlates with the generally observed LSFL periodicities^{4,22,68}. A quantitative study of the variation of the SPP periodicity with laser fluence is now presented, and compared to the LSFL ripples formed using a very low number of laser pulses.

Figure 7 shows both theoretical and experimental periodicities. The period of the LSFL structures is presented as a function of laser fluence, for 100 fs pulse duration. When SPP resonance conditions are satisfied, the resulting SPP period tends to the laser wavelength when increasing laser fluence. In the optically active range (fluence is greater than 0.7 J/cm^2 and pulse duration $\tau = 100 \text{ fs}$), the calculation results agree with the presented experimental measurements taken from Refs^{4,68,74} at very low number of pulses. The single pulse case is explained by excitation of SPP via coupling with a surface

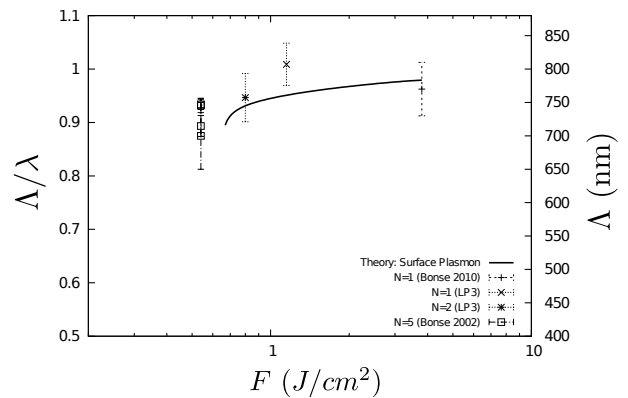


FIG. 7: Experimental measurements of the LSFL periods, as a function of laser fluence. $\tau = 100 \text{ fs}$, $\lambda = 800 \text{ nm}$, $\theta = 0^\circ$. The periods resulting from theoretical investigations are also represented. Bonse (2010) refers to Ref.⁴ and Bonse (2002) to Ref.⁶⁸

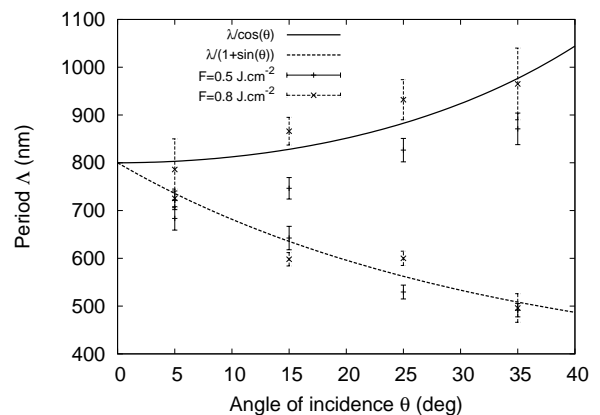


FIG. 8: Ripple periodicity as a function of angle of incidence and laser polarization after 10 laser pulses. Pulse duration is 100 fs, and laser wavelength is 800 nm.

defect. The case $N = 2$ is explained by coupling with roughness. This result shows that the periodicity of Surface Plasmon Polaritons well describes the evolution of the structure period as a function of laser fluence at reduced pulse number.

In the case of 10 laser pulses, LSFL ripples are well-developed, and scattering by a grating model well explains the observed periodicities, which confirms Ref⁷⁵. Figure 8 shows the comparison between theoretical variation of period with angle of incidence with experiments made using 10 pulses at various fluences^{72,74}. Both directions of polarization are presented. The theory of scattering by a periodically structured surface leads to a periodicity given by⁶²

$$\Lambda_P = \frac{\lambda}{\sqrt{\eta^2 - \sin^2 \theta}}$$

where $\eta = \sqrt{\frac{\varepsilon_1 \varepsilon_2}{\varepsilon_1 + \varepsilon_2}}$. $\eta \sim 1$, $\Lambda_P \sim \frac{\lambda}{\cos \theta}$ for polarization

parallel to the plane of incidence. For S polarization,

$$\Lambda_S = \frac{\lambda}{\eta + \sin \theta}$$

The variations of both measured and calculated ripple periods are explained by the variation of η near the critical density. Actually, $\eta \sim 1$ if $Re(\epsilon) \ll -1$, and η varies between 0.5 and 1.5 if the condition (Eq. 9) is satisfied. This section demonstrated that the theory of SPP excitation on gratings agrees with the experiments and explains the variation of the ripple period with the angle of incidence and with laser polarization. Such a modulation arises after several pulses. Several initial laser pulses generate roughness. The next pulses excite SPPs by coupling with surface roughness and defects, then the interference of SPP with laser pulse leads to periodic modulation of the energy in the time scale of the laser pulse. Thus, a periodic phase transition is achieved by electron-phonon coupling, and leads to the structuring of the surface, following a pattern given by SPP periodicity.^{71,76} We underline that the threshold fluence allowing SPP resonance on the surface of a grating is decreased with respect to the results presented in Figure 2 (a), since the energy absorption is enhanced in the presence of the grating⁶¹.

VI. CONCLUSIONS

The possibility of the surface plasmon polariton excitation on Si surface irradiated by a femtosecond laser pulse has been theoretically demonstrated. A sufficient number of free-carriers is excited from the valence band to the conduction band during the laser pulse, thus satisfying the SPP excitation conditions. The required ranges of laser fluences and pulse durations have been identified to satisfy the SPP excitation conditions. In particular, SPPs can be excited by using a femtosecond laser with 800 nm wavelength, 100 fs pulse duration and with laser fluences larger than $0.7 J/cm^2$. As a result, a thin layer is excited, with a lifetime longer than the pulse duration and with a depth of several tens of nanometers. The threshold intensity required to excite SPPs is higher with a sub-100 fs pulse duration than with a pulse duration longer than 100 fs. This effect is due to the free-carrier diffusion induced by strong gradients of free-carrier density and energy, enhanced at low pulse duration, and to the increase of surface reflectivity which limits the absorbed energy at short pulse duration.

Furthermore, a comparison of the calculated SPP periodicities and experimentally measured ripple periodicities allows us to conclude that the formation of periodic structures with a reduced number of laser pulses is due to the excitation of SPPs at the Si surface.

The presence of a surface roughness with $\delta \ll \lambda$ leads to the coupling of the laser wave with the roughness. We have found that the required roughness amplitude allowing the coupling of laser wave with the surface is 8 nm. It

is also possible to obtain periodic structures by scattering on defects ($\delta \sim \lambda$) that are present at the surface by excitation of localized surface plasmon polaritons. These results underline the importance of the surface quality in the SPP excitation and thus to the LSFL ripple formation.

As a result of the performed analysis, the possibilities of control over the period of the LSFL ripples can be deduced in the regime of low number of pulses. The period can be reduced down to 40% by increasing the angle of incidence for S polarization from normal incidence to 40° incidence, and can be increased up to 37% by increasing the angle of incidence for P polarization from normal incidence to 40° of incidence. The period of the LSFL ripples can be increased of 10% by increasing the laser fluence from excitation threshold $0.7 J/cm^2$ up to $5 J/cm^2$. Finally, the period of the LSFL structure is shown to be reduced with the number of laser pulses and can be decreased by 50 % with respect to the one obtained for a single pulse. However, the corresponding mechanism is still under discussions^{4,25}. Our calculation results have thus demonstrated the existence of the lower fluence limit, below which the surface plasmon polaritons can not be excited on Si. In addition, the model has an upper fluence limit above which the band structure is destroyed and the material is severely damaged or ablated. Taking into account that for ripple formation, laser wave should enter in resonance with SPP wave, we confirm the fact that there is a well-defined fluence window for ripple formation due to SPP²², which depends on laser wavelength and pulse duration. For the considered parameters, fluence is in the range between $0.7 J/cm^2$ and $5 J/cm^2$.

ACKNOWLEDGMENTS

TJD is grateful to the French Ministry of Research for the PhD grant. The National Computational Center for Higher Education (CINES) under project c2011085015 is acknowledged.

- ¹M. Birnbaum. *Journal of Applied Physics* **36**, 11, p. 3688 (1965).
- ²J. F. Young, J. Preston, H. V. Driel, and J. Sipe. *Physical Review B* **27**, p. 2 (1983).
- ³I. Ursu, I. Mihailescu, L. Nistor, V. Teodorescu, A. Prokhorov, V. Konov, and V. Tokarev. *Applied Optics* **24**, p. 22 (1985).
- ⁴J. Bonse and J. Krüger. *Journal of Applied Physics* **108**, p. 034903 (2010).
- ⁵G. Tsididis, E. Stratakis, and K. Aifantis. *Journal of Applied Physics* **111**, p. 053502 (2012).
- ⁶J. Renger, R. Quidant, N. van Hulst, S. Palomba, and L. Novotny. *Physical Review Letters* **103**, p. 266802 (2009).
- ⁷A. Borowiec. *Applied Physics Letters* **82**, p. 25 (2003).
- ⁸J. Bonse, M. Munz, and H. Sturm. *Journal of Applied Physics* **97**, p. 013538 (2005).
- ⁹A. Vorobyev and C. Guo. *Journal Of Applied Physics* **104**, p. 063523 (2008).
- ¹⁰T. Crawford and H. Haugen. *Applied Surface Science* **253**, pp. 4970–4977 (2007).
- ¹¹A. Vorobyev. *Journal of Applied Physics* **104**, p. 053516 (2008).

- ¹²A. Vorobyev and C. Guo. *Applied Physics Letters* **92**, p. 041914 (2008).
- ¹³J. Reif, F. Costache, M. Henyk, and S. V. Pandelov. *Applied Surface Science* **197-198**, pp. 891–895 (2002).
- ¹⁴A. Ben-Yakar, A. Harkin, J. Ashmore, R. Byer, and H. Stone. *Journal of Physics D: Applied Physics* **40**, p. 1447 (2007).
- ¹⁵O. Varlamova, F. Costache, M. Ratzke, and J. Reif. *Applied Surface Science* **253**, pp. 7932–7936 (2007).
- ¹⁶T. Her, R. Finlay, C. Wu, S. Deliwala, and E. Mazur. *Applied Physics Letters* **73**, p. 12 (1998).
- ¹⁷J. E. Carey, C. H. Crouch, and E. Mazur. *Optics and Photonics News* **14**, p. 2 (2003).
- ¹⁸T. Sarnet, R. Torres, V. Vervisch, P. Delaporte, M. Sentis, M. Halbax, J. Ferreira, D. Barakel, M. Pasquinielli, S. Martinuzzi, L. Escoubas, F. Torregrosa, H. Etienne, and L. Roux. *ICALEO 2008 Congress Proceedings* **101**, p. 161 (2008).
- ¹⁹J. Reif, O. Varlamova, M. Ratzke, M. Schade, H. Leipner, and T. Arguirov. *Applied Physics A* **101**, p. 361 (2010).
- ²⁰J. Sipe, J. F. Young, J. Preston, and H. V. Driel. *Physical Review B* **27**, p. 2 (1983).
- ²¹J. Skolski, G. Römer, J. Obona, V. Ocelik, A. H. in't Veld, and J. T. M. D. Hosson. *Physical Review B* **85**, p. 075320 (2012).
- ²²J. Bonse, A. Rosenfeld, and J. Krüger. *Journal of Applied Physics* **106**, p. 104910 (2009).
- ²³F. Costache. *Applied Physics A* **79**, p. 1429 (2004).
- ²⁴J. Reif, M. Ratzke, O. Varlamova, and F. Costache. *Materials Science and Engineering B* **134**, pp. 114–117 (2006).
- ²⁵G. Tsididis, M. Barberoglou, P. Loukakos, E. Stratakis, and C. Fotakis. *Physical Review B* **86**, p. 115316 (2012).
- ²⁶M. Guillermin, F. Garrelie, N. Sanner, E. Audouard, and H. Soder. *Applied Surface Science* **253**, pp. 8075–8079 (2007).
- ²⁷G. Miyaji and K. Miyazaki. *Optics Express* **16**, p. 20 (2008).
- ²⁸M. Huang, F. Zhao, Y. Cheng, N. Xu, and Z. Xu. *ACS Nano* **3**, p. 12 (2009).
- ²⁹S. Sakabe. *Physical Review B* **79**, p. 033409 (2009).
- ³⁰F. Garrelie, J. Colombier, F. Pigeon, S. Tonchev, N. Faure, M. Bounhalli, S. Reynaud, and O. Parriaux. *Optics Express* **19**, p. 10 (2011).
- ³¹H. Raether. *Surface plasmons on smooth and rough surfaces and on gratings* (Springer-Verlag, 1986).
- ³²A. Zayats, I. Smolyaninoy, and A. Maradudin. *Physics Reports* **408**, pp. 131–314 (2005).
- ³³J. Bonse, A. Rosenfeld, and J. Krüger. *Applied Surface Science* **257**, pp. 5420–5423 (2011).
- ³⁴B. Hecht, H. Bielefeldt, L. Novotny, Y. Inouye, and D. Pohl. *Physical Review Letters* **77**, p. 9 (1996).
- ³⁵K. Sokolowski-Tinten, J. Bialkowski, A. Cavalleri, D. V. D. Linde, A. Oparin, J. M. ter Vehn, and S. Anisimov. *Physical Review Letters* **81**, p. 1 (1998).
- ³⁶K. Sokolowski-Tinten and D. von der Linde. *Physical Review B* **61**, p. 4 (2000).
- ³⁷J. Bok and M. Combescot. *Physical Review Letters* **47**, p. 21 (1981).
- ³⁸H. V. Driel. *Physical Review B* **35**, p. 15 (1987).
- ³⁹T. Sjodin, H. Petek, and H.-L. Dai. *Physical Review Letters* **81**, p. 25 (1998).
- ⁴⁰E. Palik. *Handbook of Optical Constants of Solids* (Academic Press, 1985).
- ⁴¹S. Sze and K. K. Ng. *Physics Of Semiconductor Devices* (Wiley-Interscience, 2007).
- ⁴²K. Thornber. *Journal Of Applied Physics* **52**, p. 279 (1981).
- ⁴³T. Y. Choi and C. P. Grigoropoulos. *Journal of Applied Physics* **92**, p. 9 (2002).
- ⁴⁴N. Bulgakova, R. Stoian, A. Rosenfeld, I. Hertel, W. Marine, and E. Campbell. *Applied Physics A* **81**, pp. 345–356 (2005).
- ⁴⁵J. Bonse, K. Brzezinka, and A. Meixner. *Applied Surface Science* **221**, pp. 215–230 (2004).
- ⁴⁶M. Fischetti and S. Laux. *Physical Review B* **38**, p. 14 (1988).
- ⁴⁷M. Born and E. Wolf. *Principles of Optics. Electromagnetic theory of propagation, interference and diffraction of light.* (Cambridge University Press, 1980), 7th edition edition.
- ⁴⁸D. Bäuerle. *Laser Processing and Chemistry* (Springer, 2000).
- ⁴⁹N. Bulgakova, R. Stoian, and A. Rosenfeld. *Quantum Electronics* **40**, p. 11 (2010).
- ⁵⁰J. Jackson. *Classical electrodynamics* (Wiley, 1999).
- ⁵¹D. Jou, J. Casas-Vazquez, and G. Lebon. *Extended irreversible thermo-dynamics* (Springer-Verlag, 1993).
- ⁵²F. Alvarez and D. Jou. *Applied Physics Letters* **90**, p. 083109 (2007).
- ⁵³B. Palpant, Y. Guillet, M. Rashidi-Huyeh, and D. Prot. *Gold Bulletin* 2008 **41**, p. 2 (2008).
- ⁵⁴P. Desai. *Journal of Chemical Reference and Datas* **15**, p. 3 (1986).
- ⁵⁵W.-K. Rhim and K. Ohsaka. *Journal of Crystal Growth* **208**, pp. 313–321 (2000).
- ⁵⁶A. L. Magna, P. Alippi, V. Privitera, G. Fortunato, M. Camalleri, and B. Svensson. *Journal Of Applied Physics* **95**, p. 9 (2004).
- ⁵⁷A. Rousse, C. Rischel, S. Fournaux, I. Uschmann, S. Sebban, G. Grillon, P. Balcou, E. Forster, J. Geindre, P. Audebert, J. Gauthier, and D. Hulin. *Nature* **410**, pp. 65–68 (2001).
- ⁵⁸S. Sundaram and E. Mazur. *Nature Materials* **1**, p. 217 (2002).
- ⁵⁹K. Sokolowski-Tinten, C. Blome, J. Blums, A. Cavalleri, C. Dieterich, A. Tarasevitch, I. Uschmann, E. Forster, M. Kammmler, M. H. von Hoegen, and D. von der Linde. *Nature* **422**, pp. 287–289 (2003).
- ⁶⁰M. Combescot and J. Bok. *Journal of Luminescence* **30**, pp. 1–17 (1985).
- ⁶¹I. Ursu, I. Mihailescu, A. Popa, A. Prokhorov, V. Konov, V. Ageev, and V. Tokarev. *Applied Physics Letters* **45**, pp. 365–367 (1984).
- ⁶²A. M. Bonch-Bruевич, M. N. Libenson, V. S. Makin, and V. A. Trubaev. *Optical Engineering* **31(4)**, pp. 718–730 (1992).
- ⁶³L. Novotny, B. Hecht, and D. Pohl. *Journal of Applied Physics* **81**, p. 4 (1997).
- ⁶⁴S. A. Maier. *Plasmonics, Fundamentals and Applications* (Springer, 2007).
- ⁶⁵V. Makin, Y. I. Pestov, R. Makin, and A. Y. Vorobyev. *Journal of Optical Technology* **76**, p. 9 (2009).
- ⁶⁶J. I. Pankove. *Optical Processes in Semiconductors* (Dover Science, 1971).
- ⁶⁷D. Hulin, M. Combescot, J. Bok, A. Migus, J. Y. Vinet, and A. Antenotti. *Physical Review Letters* **52**, p. 22 (1984).
- ⁶⁸J. Bonse, S. Baudach, J. Krüger, W. Kautek, and M. Lenzner. *Applied Physics A* **74**, pp. 19–25 (2002).
- ⁶⁹D. Korfiatis, K. Thoma, and J. Vardaxoglou. *Journal of Physics D: Applied Physics* **40**, p. 6803 (2007).
- ⁷⁰A. D. Bristow, N. Rotenberg, and H. M. V. Driel. *Applied Physics Letters* **90**, p. 191104 (2007).
- ⁷¹T. J.-Y. Derrien, R. Torres, T. Sarnet, M. Sentis, and T. Itina. *Applied Surface Science* **258**, p. 23 (2012).
- ⁷²T. J.-Y. Derrien. *Nanostructuration de cellules photovoltaïques par impulsion laser femtoseconde. Étude des mécanismes de formation*. Ph.D. thesis, Université de la Méditerranée - Aix Marseille II (2012).
- ⁷³Lumerical. FDTD Solutions, <http://www.lumerical.com>.
- ⁷⁴R. Torres. *Structuration du silicium par laser femtoseconde : application au photovoltaïque*. Ph.D. thesis, Université de la Méditerranée (2011).
- ⁷⁵A. A. Ionin, S. I. Kudryashov, S. Makarov, L. Seleznev, D. Sinityn, E. Golosov, O. A. Golosova, U. Kobolov, and A. Ligachev. *Applied Physics A* **107**, pp. 301–305 (2012).
- ⁷⁶J. Colombier, F. Garrelie, N. Faure, S. Reynaud, M. Bounhalli, E. Audouard, R. Stoian, and F. Pigeon. *Journal Of Applied Physics* **111**, p. 024902 (2012).

LIST OF FIGURES

1	Real part of the dielectric function of Si $\varepsilon(\omega) = \left(\frac{k\epsilon}{\omega}\right)^2$ as a function of photon energy compared to the plasma frequency $\omega_p = \sqrt{\frac{n_e e^2}{m_e \epsilon_0}}$. If the plasma frequency is located on the left of the resonance peak, surface mode is not bounded to the surface and SPP are not allowed. If the plasma frequency is located on the right of the surface plasmon polariton resonance peak, the SPPs are allowed.	5
2	(a) Minimum of the real part of the dielectric function as a function of laser fluence. Blue line indicates the threshold for SPP excitation e.g. $\Re(\varepsilon) = -1$. (b) Maximum of the reached density during the interaction as a function of laser fluence. Blue line indicates critical density e.g. $\Re(\varepsilon) = 0$. $n_{cr} = 4.29 \times 10^{21} \text{ cm}^{-3}$. Several laser pulse durations are represented.	6
3	Fluence threshold for SPP resonance as a function of pulse duration.	6
4	Distribution of the dielectric function as a function of depth and time. $\tau = 50 \text{ fs}$, $F = 0.62 \text{ J/cm}^2$	7
5	Transmitted field amplitude below the selvedge region of Si. Roughness amplitude is (a) $\delta = 0 \text{ nm}$, (b) $\delta = 8 \text{ nm}$, (c) $\delta = 15 \text{ nm}$ at wavelength 800 nm. In these simulations, $\varepsilon = \varepsilon_\infty = 13.64 + 0.048i$	7
6	Wavelength normalized period of SPP as a function of free-carrier density at vacuum - Si interface when the conditions of resonance are met.	8
7	Experimental measurements of the LSFL periods, as a function of laser fluence. $\tau = 100 \text{ fs}$, $\lambda = 800 \text{ nm}$, $\theta = 0^\circ$. The periods resulting from theoretical investigations are also represented. Bonse (2010) refers to Ref. ⁴ and Bonse (2002) to Ref. ⁶⁸	8
8	Ripple periodicity as a function of angle of incidence and laser polarization after 10 laser pulses. Pulse duration is 100 fs, and laser wavelength is 800 nm.	8